

# Measurements of entrainment characteristics of swirling jets

S. H. PARK and H. D. SHIN†

Department of Mechanical Engineering, Korea Advanced Institute of Science and Technology,  
371-1, Kusong-dong, Yusong-gu, Taejeon, 305-701, Korea

(Received 25 November 1992 and in final form 16 March 1993)

**Abstract**—Entrainment characteristics of free swirling jets were investigated by the schlieren flow visualization and the newly contrived technique for measuring the entrainment velocity, which is demonstrated to be reasonably accurate and reliable. The visualization studies reveal that the entrainment rate increases with the swirl intensity. Schlieren photographs, which were synchronized with the fluctuation velocity signal, display that the precessing vortex core (PVC) induces large scale periodic motion in the jet boundary regions near the nozzle exit. The PVC effect on entrainment is scrutinized by employing two swirling jets, one with a PVC and the other with a substantially suppressed PVC. The results clearly indicate that the entrainment is enhanced considerably due to the PVC. For swirl number  $S < 0.6$ , the entrainment rate is fairly independent of the Reynolds number ( $Re$ ) and increases more or less nonlinearly with the downstream region, while, for  $S > 0.6$ , it becomes higher with  $Re$ ; this is due to the fact that the high-frequency PVC is induced at higher Reynolds number.

## 1. INTRODUCTION

SWIRLING has been effectively utilized in a large number of practical combustion devices. Numerous studies, both experimental and theoretical, on the principal characteristics of swirl have been documented [1]. These investigations have established that swirl has a significant impact on the global flow and thermal fields; the jet growth, entrainment and decay in isothermal flows, flame shape, stability and combustion intensity for reacting flows, to name a few, are examples of such characteristics.

Despite the wide-spread use of swirl in practical systems, a comprehensive understanding of the underlying physics is still incomplete; proper formulation and modeling of the swirling flow phenomena needs further concerted efforts. In particular, serious endeavors are required to portray large-scale periodic motions, which are often observed in strongly swirling flows at high Reynolds numbers [2]. These motions are customarily referred to as the precessing vortex core (PVC). The PVC is believed to play a dominant role in determining the main characteristics of swirling flows [1]. The preceding works [1] pointed out that the frequency and intensity of PVC depend on the flow conditions as well as on the combustion states. It is important to recognize that the flow in the region where PVC appears is not axisymmetric; the motion displays a three-dimensional, time-dependent, large-scale coherent structure. As is well known, the entrainment rate of ambient fluid into turbulent shear flow is of primary relevance in combustion studies. In many realistic systems, the entrainment rate is strongly

influenced by the presence of large-scale structures in the boundary regions [3]. Therefore, it is of prime interest to inquire into the possibility that the PVC can induce large-scale eddy motions, which, in turn, as asserted above, would substantially affect the entrainment rate.

In the present work, extensive experimental investigations are undertaken to address the above-stated behavior of PVC and eddy motions in the boundaries. Specifically, detailed descriptions will be made of the PVC, which exists at the nozzle exit. The major purpose of the present paper is to show that the PVC produces large-scale eddy motions around the interface between the turbulent and non-turbulent regions (surroundings). It should be noted that, in the present study, attention is focused mainly on the near field of the nozzle exit. Furthermore, it will be demonstrated that these large-scale eddies substantially enhance the entrainment rate of swirling flows.

Both the flow visualization technique and the direct measurements of entrainment velocities in the vicinity of a flat plate were implemented in order to identify the influence of the PVC on the entrainment; experiments were performed for two typical cases with the identical inlet conditions. In one case, a strongly swirling jet, which contains the PVC, is adopted (isothermal flow). For the other case, an extremely small flame was introduced into the central region inside the air nozzle of the swirler. By this method, the PVC was suppressed; however, no other serious alterations, such as an increase of air temperature, were observed in the flow conditions. Careful measurements of the entrainment were secured for these two cases. These experimental results will, therefore, clarify the relationship between the PVC and the entrainment rate.

† To whom correspondence should be addressed.

## NOMENCLATURE

$D$	inner diameter of air nozzle	$U$	time mean axial velocity component
$L$	length of air nozzle	$V$	time mean radial velocity component
$M$	mass flowrate at the arbitrary cross-section	$V_i$	entrained velocity at the measurement point $i$
$M_e$	mass flowrate of entrained ambient air	$x$	axial distance from the exit of air nozzle
$M_o$	total mass flowrate through swirl generator	$X_j$	$j$ th axial cross-section
$Re$	Reynolds number based on air nozzle diameter, $D$	$\Delta x$	interval between $j$ th and $j+1$ th axial cross-section.
$R_i$	radial distance from jet axis to measurement point $i$	Greek symbols	
$r$	radial distance from jet axis	$\rho$	air density
$S$	swirl number	$\Psi$	nondimensional entrainment ratio.

## 2. EXPERIMENTAL APPARATUS AND PROCEDURES

## 2.1. Apparatus

A vertically-mounted Ijmuiden type swirl burner [4] was used to generate isothermal swirling jets. As shown schematically in Fig. 1, experiments were conducted for swirling air jets into the ambient air. The swirl burner consists of movable blocks, fixed blocks, an air nozzle, a fuel nozzle and a swirl controller. An end plate of 400 (mm) diameter was attached to the exit of the sharp-edged round air nozzle, the size of which is 30 mm in inner diameter ( $D$ ) and 75 mm in length ( $L$ ). In the present experiment, by attaching the end plate, the axial component of entrainment was appreciably reduced near the nozzle exit. Consequently, the entrainment was primarily controlled by a single component of velocity, i.e. the component in the radial direction. The fuel nozzle, located at the center of the air nozzle, was of outer and inner diameters of 2 and 1.6 mm, respectively. The fuel nozzle

was mounted concentrically to the air nozzle through all the experiments. Commercial-grade propane gas was used as fuel. Isothermal swirling air supplied by an air blower was introduced into an air distributor and was fed into the swirler through eight air inlet ports.

The swirl intensity of the jet can be controlled by adjusting the angle of the movable blocks mounted in the air passage relative to the fixed blocks. The swirl number ( $S$ ), representing the swirl intensity, is conventionally defined as the ratio of the angular momentum to the axial momentum, multiplied by the radius of the air nozzle. Direct measurements of the swirl number are usually complicated and tedious; however, in the case of a movable block type swirl generator, it can be estimated by theoretical calculations based on the geometric parameters of the swirl generator [5]. All the swirl numbers used in this study were calculated according to the theoretical method described by Beer and Chigier [5].

The flow rate of supplied air can be altered over a wide range. By this method, the Reynolds number ( $Re$ ) based on the air nozzle exit diameter ( $D$ ) was varied accordingly.

## 2.2. Flow visualization methods

*Single-shot schlieren photographs.* Instantaneous schlieren photography was employed in order to visualize the eddy motions in the swirling flow boundary region, the angle of spread, and the entrainment characteristics of the swirling jets. An externally controlled xenon-arc lamp with a flash duration of 3  $\mu$ s and light intensity of  $11 \times 10^6$  candela was used as the spark light source. For schlieren photography, the air supplied to the coaxial jet was preheated, up to a temperature of about 30°C higher than the ambient air, with a hydrogen burner installed in the piping of supplied air. The temperature increase of this magnitude gives rise to measurable density variations of air. To visualize the entrainment of the surrounding air into the jet in the near-nozzle exit region, a locally coiled electric resistance wire was located outside the

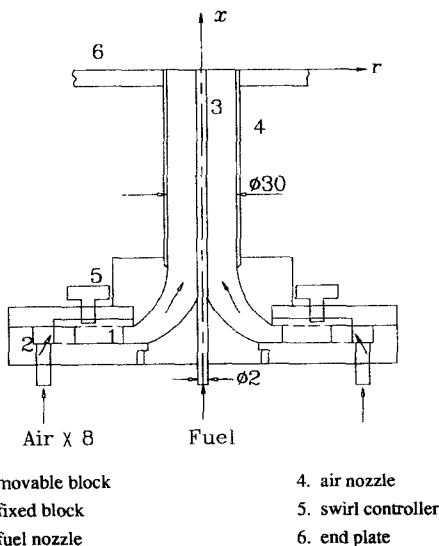


FIG. 1. Arrangement of the swirling burner of the present experimental set-up.

boundary of the swirling jet; this induced a small density gradient in the entrained air. Detailed visualizations in the present study were confined to the near-nozzle region of about five air nozzle diameters in the streamwise distance.

*Visualization of the periodic phenomena.* In most visualization studies of periodic motions in strongly swirling flow fields, a high-speed cinematographic system has been used. However, a serious disadvantage of this system is that a continuous and intensive light source is required to obtain high-quality pictures for a very short time-exposure. Therefore, in the present study, a simple synchronizing system was contrived, as depicted in Fig. 2. This is composed of the conventional schlieren system, the hot wire anemometer (HWA), and the electronic circuit which detects the timing of camera shutter action. The operational principle of the system is as follows. The fluctuating velocity signals, which are detected by HWA located at the boundary region between the swirling jet and ambient air, are continuously stored by a tape recorder (HP, 3968A). The strobo slave (Genrad, 1539A) was triggered to flash a Xenon lamp, in synchronization. The schlieren image of the flow phenomena occurring near the nozzle exit region was photographed at that instant with a still camera. The output signal of the shutter action from the electronic circuit was recorded, in conjunction with the fluctuating velocity signal, on the magnetic tape recorder. In order to check the quality of these signals, they are continuously monitored on an oscilloscope (HP, 1744A) during the entire course of the experiment. Analyses

of the schlieren photographs and post-processings of the recorded signals allowed detailed examinations of the salient characteristics of PVC motions.

### 2.3. Entrainment measurement techniques

*Previous methods.* Prior experimental measurements of entrainment have mostly been for weakly swirling flows; measurement data for strongly swirling flows are scarce [1]. In general, there are several measurement techniques of entrainment for both the swirling and the non-swirling jet. These are:

- (a) integration of the radial profiles of time-mean axial velocity,
- (b) interception method of the plume by a horizontal ceiling layer at a fixed height,
- (c) Ricou-Spalding's direct measurement technique.

Brief descriptions of the above techniques are given below. Delichatsios and Orloff [6] discussed in detail several problems associated with the application of the above methods to free turbulent non-swirling jets with and without reaction. These include the inaccuracies in defining the edge of a free turbulent jet. More specifically, difficulties arise in measuring the variable density in the flow field with chemical reaction (method (a)), eliminating the effects of ambient drafts on the entrainment (method (b)), and the suppression of small and large scale eddies which might affect the entrainment processes by confining the original flow field locally (method (c)). The majority of the previous measurements of the entrainment rate

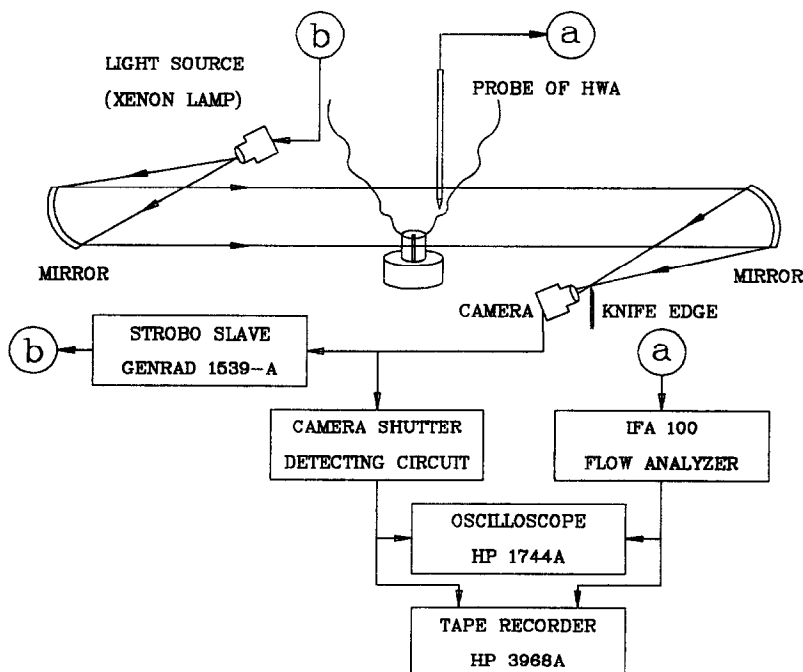


FIG. 2. Schematic diagram of the hot-wire anemometer/schlieren synchronizing system.

for the swirling jet have been made by using the integration method [7–9]. Furthermore, most of these preceding measurements were performed for weakly swirling jets with no internal recirculation ( $S < 0.6$ ). In the case of strongly swirling jets ( $S > 0.6$ ), several features are noticeable: intermittency of the flow is more conspicuous; a recirculation zone exists; and the jet spreads with larger angles. In view of these complex flow features, straightforward applications of the above methods are less effective for strongly swirling jets. In particular, due to the notable intermittency of the flow, the results obtained by the integration method (a) become unreliable and inaccurate for a strongly swirling flow. Therefore, in the present study, a new method was proposed to measure the entrainment rate.

*The present method.* Paraffin smoke wires are installed near the exit of the jet nozzle as shown in Fig. 1. The direction of the ambient air flow drawn into the swirling jet was studied by taking photographs of the smoke lines. Figure 3(a) presents an example of such photographs, illustrating the flow field in the axial cross-section at  $x/D = 0.5$ , viewed from the downstream side for the isothermal case of  $S = 1.87$  and  $Re = 20\,500$ . These streaklines indicate that the ambient air far away from the swirl jet boundary is entrained almost radially towards the axis of the swirling jet even at a high swirling ratio, since the entrainment in the axial direction is blocked by the

end plate, as remarked earlier. In Fig. 3(b), it is clearly seen that the surrounding air moves radially inward in the horizontal direction normal to the axis of the jet. In the near-exit ambient region, it is evident that the axial velocities ( $U$ ) are negligibly small. This observation is consistent with the results of visualization by other work [10], which was conducted for a free non-swirling jet issued with an end plate attached at the nozzle exit.

The continuity equation for the time-mean swirling flow field can be written in cylindrical coordinates as follows:

$$\frac{\partial U}{\partial x} + \frac{1}{r} \frac{\partial(rV)}{\partial r} = 0 \quad (1)$$

where  $U$  and  $V$  represent the time-mean axial and radial velocities, respectively. Since  $U \cong 0$  in the entrained surrounding air flow field, as observed in Fig. 3(b), the above yields

$$\frac{1}{r} \frac{\partial(rV)}{\partial r} \cong 0, \quad \text{that is, } rV \cong \text{constant}. \quad (2)$$

From this relation,  $V$  can be regarded as the total entraining velocity of ambient air since  $U \cong 0$  in this region. Now, direct measurements of the radial velocity  $V$  of ambient air entrained into the swirling jet may be performed by using an anemometer. The entrainment rate is readily calculated by using the measured velocity data. Since the flow direction can be assumed to be radial (where equation (2) is applicable), the full velocity vector can be constructed by acquiring the information only on the absolute magnitude of the velocity.

A precision Tr-Type anemometer (Rion Co., AM-03) was employed to measure only the magnitude of the velocity. The range of measurement is from  $0.05$  to  $3 \text{ m s}^{-1}$ , and the accuracy is within 2% of the measured value without the directional resolution. The velocity data at any given point were obtained by averaging six sets of repeated measurements. Each data set was secured over a time span of 10 s. Reproducibility of the measured velocity data was found to be satisfactory within the uncertainty interval  $\pm 4\%$  [11]. The region of velocity measurements is exemplified schematically in Fig. 4. The region is divided into two main parts, i.e. one is the turbulent region inside the swirling jet injected into the stagnant air, and the other is the non-turbulent region outside the first one. The measurement points are located in the non-turbulent region. At two neighboring measurement points in the non-turbulent region at a cross-section ( $X_j$ ), the following relation, derived from equation (2), holds:

$$R_i V_i = R_{j+1} V_{j+1} \quad (3)$$

where  $R_i$  and  $V_i$  represent the radial distance from the axis to the measurement point  $i$  and the entraining velocity in the radial direction at that point, respectively. In order to establish the local entrainment rate

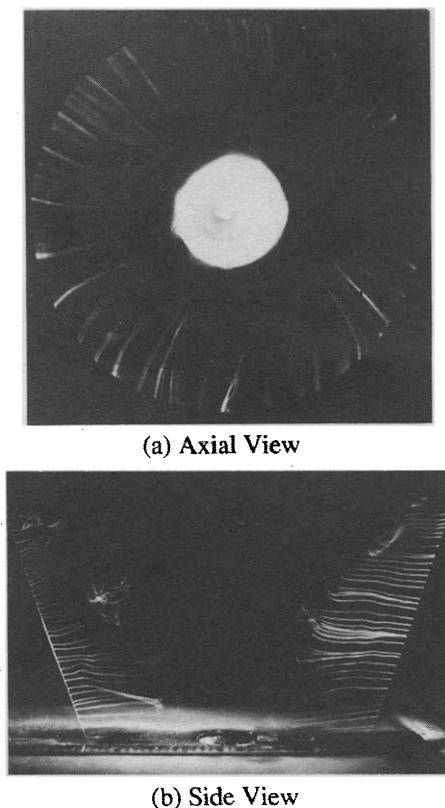


FIG. 3. Smoke line visualizations of the air entrainment. Conditions are  $Re = 20\,500$  and  $S = 1.87$ . (a) Axial view. (b) Side view.

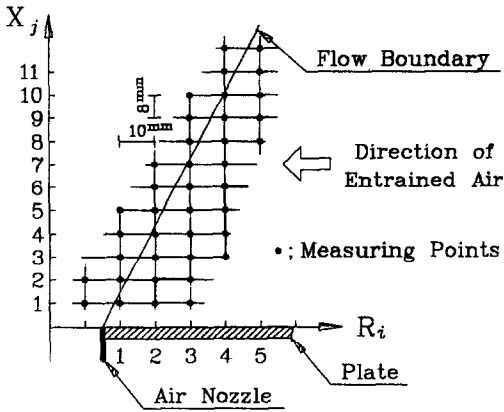


FIG. 4. Coordinate system and measuring locations for the entrainment measurements.

at a given axial station (say at the axial cross-section  $X_j$ ), the following procedure was taken. By inspecting the entire sets of velocity measurement data, the approximate location of the demarcation of the region in which equation (2) is applicable is determined (see Fig. 4). The entrained air velocity ( $V_c$ ) obtained at the measurement points closest to this demarcation line ( $R_c$ ) will be used to estimate the entrainment rate. Therefore, the local entrainment rate at the axial station  $X_j$  can be calculated:

$$\frac{dM_c}{dx} = 2\pi\rho R_{c_j} V_{c_j}. \quad (4)$$

The rationale of choosing the data at  $R_c$  is obvious. Since  $V$  is inversely proportional to  $r$ , the largest entrainment velocity is obtainable at  $R = R_c$ . At large radii, the magnitude of  $V$  decreases; this implies that the contaminations by external disturbances become comparatively more conspicuous. By utilizing the data at small radii ( $R = R_c$ ), the measurement error of entrainment will be minimized.

In view of equation (4), the entrainment rate at the axial station  $X_j$  can be expressed as

$$M_c = 2\pi\rho\Delta x \sum_{j=1}^n R_{c_j} V_{c_j}. \quad (5)$$

Consequently, the total mass flow rate  $M$  is the sum of the entrainment  $M_c$  and the initial mass flow rate of the jet issued from the nozzle  $M_o$ :

$$M = M_c + M_o. \quad (6)$$

In accordance with the conventional definition, the nondimensional entrainment rate  $\Psi$  can be defined as

$$\Psi = \frac{M_c}{M_o} = \frac{M}{M_o} - 1. \quad (7)$$

### 3. RESULTS AND DISCUSSION

#### 3.1. Flow visualization

First, the qualitative effect of swirl on the gross flow characteristics is illustrated in Fig. 5 ( $Re = 20\,500$ ). The effect of swirl on the spreading angle of the jet is quite noticeable. It is discernible that, at larger swirl numbers, the indentation of the turbulent/non-turbulent interface is more conspicuous, and large-scale protrusions in this region are visible. Such large scale eddies are expected to play a main role in the entrainment processes [3]. Therefore, it is anticipated that the swirl will have substantial influence on the entrainment rate. In particular, in the case of a strongly swirling jet, it is remarkable that a large scale eddy motion appears immediately after the air nozzle exit, as exhibited in Fig. 5(c). In the next section, the periodicity of such large eddy motions will be discussed in connection with the PVC motion which often occurs in strong swirling flows. Horizontally-oriented bright and dark bands in photographs are observed in the non-turbulent region. These are generated due to the density change, which is caused when the entrained air passes through the electrically heated coiled-wire. This provides other evidence to the earlier argument that the ambient air entrainment moves almost horizontally inward in the vicinity of the nozzle exit ( $U \cong 0$ ).

*Relationships between large scale eddy motion and the PVC.* In an effort to understand the structure of PVC, spectral analyses of the hot wire velocity fluctuation in the region within the jet have been performed. This exercise was conducted to examine the

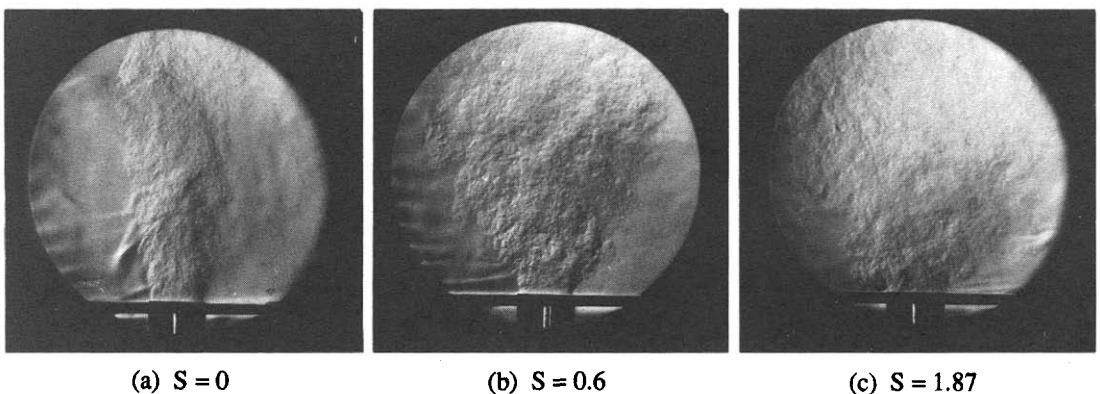


FIG. 5. Schlieren photographs of swirling jets.  $Re = 20\,500$  (a)  $S = 0$ , (b)  $S = 0.6$ , (c)  $S = 1.87$ .

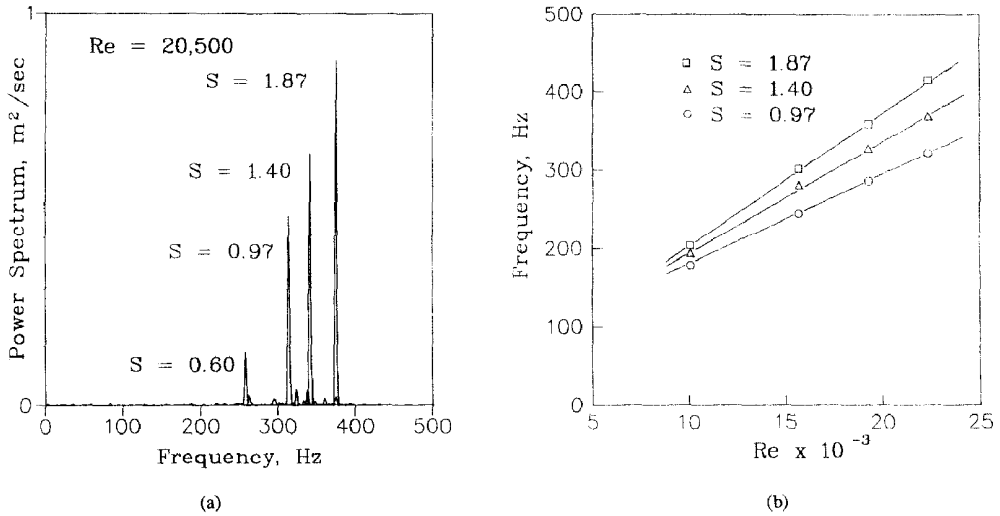


FIG. 6. Exemplary results of spectrum analyses.

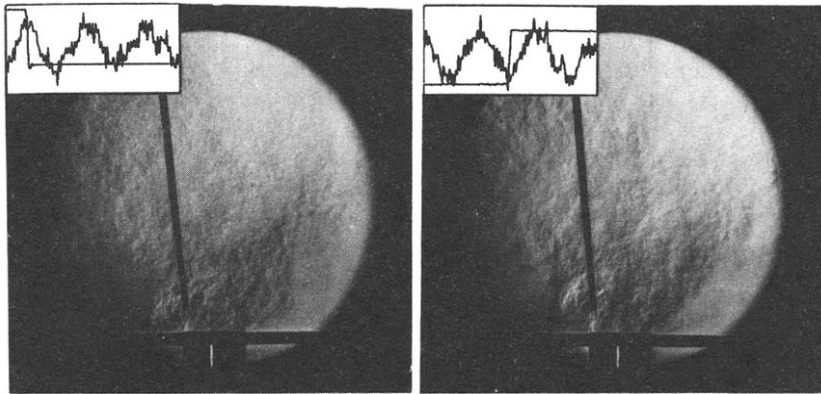
possible interrelation between large-eddy motions and PVC. An I-type hot-wire probe was used to measure the velocity in HWA. In the case of  $Re = 20\,500$ , as demonstrated in Fig. 6(a), the existence of PVC is confirmed by the presence of the dominant frequencies. For strongly swirling flows ( $S > 0.6$ ), both the intensity of power spectrum and the values of the dominant frequencies increase as  $S$  increases. However, for weakly swirling flows ( $S < 0.6$ ), the dominant frequencies do not appear. Figure 6(b) also shows that the values of the dominant frequencies increase with the Reynolds number in the case of strong swirls. As is well known, in the case of strong swirl, the presence of the dominant frequencies indicates the existence of PVC [1].

It is now of interest to inquire into the interrelation between the PVC motion and large-scale eddy motions which are observed intermittently in the vicinity of nozzle exit. A large number of instantaneous schlieren photographs were randomly taken by using the synchronizing technique for visualization described in an earlier section for the isothermal swirling flows with  $Re = 20\,500$  and  $S = 1.87$ . The flow characteristics in various phases of the fluctuating velocity signal can be identified by comparing the tape-recorded synchronized signals with the corresponding schlieren photographs. Extensive comparisons were made of the schlieren photographs and corresponding synchronized signals. It was confirmed that all the photographs taken in the same phase of the fluctuating velocity signal display consistent flow patterns at the next nozzle exit region of interest. Two typical synchronized signals of the HWA, together with the camera shutter output and the corresponding schlieren photos, are presented in Fig. 7(a). In this figure, left and right photos were taken at the instants of minimum and maximum points of the periodic velocity signals with large amplitude, respectively. In particular, it is noticeable that a large scale eddy

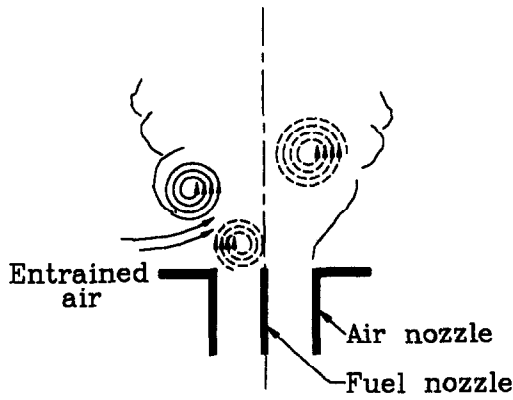
motion (engulfment) is clearly observed near the nozzle exit at which the hot wire probe is located, but this happens only when photographs were taken close to both peaks (minimum and maximum points) of the periodic velocity signal. The visualization studies disclose that large-scale eddies are shed while these are rotating in the circumferential direction near the nozzle exit. Strong engulfments are generated in the shedding zone, and the temporal period of the engulfments appears to be close to that of the PVC.

The experimental findings of Gupta *et al.* [1], by using visualization methods in the water tunnel, showed that the PVC moves downstream in the radial-tangential direction inside the swirler. Furthermore, Gupta *et al.* [1] revealed that, at the nozzle exit, an associated instability develops; a series of eddies with the radial-axial direction are shed in a manner similar to the Karman vortex street. This is different from the direction of PVC motion which is radial-tangential. The PVC motion, on the other hand, is rapidly dissipated within a distance of approximately one nozzle diameter. The present observations clearly indicate that the large eddies, which are aligned in the radial-axial direction, shed at the nozzle exit due to the PVC produce correspondingly large-scale motions on the flow boundaries of the near-exit region. It is also to be noted in Fig. 7(b) that the large eddies shed inside the swirling flows rotate inward in the radial-axial direction, but the aforementioned large scale motions on the flow boundaries rotate outward. In summary, the rotational directions of these two flow components are opposite to each other, however, the frequencies are close to each other, being approximately 300 Hz under the present experimental conditions.

For the purpose of scrutinizing the visual effect of PVC motion on the entrainment processes of the surrounding air to the swirl jet, it is highly desirable to control the PVC motion. By systematically comparing the entrainments for two cases with and without PVC.



(a)



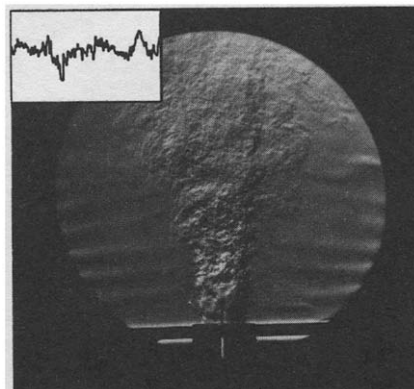
(b)

FIG. 7. (a) Signals of velocity fluctuations synchronized with the camera and the corresponding schlieren photographs without combustion. Conditions are  $Re = 20\,500$  and  $S = 1.87$ . (b) Sketch of the induced eddies at the nozzle exit. The dotted line indicates the PVC motion shed at Karman vortex street [1] and the solid line display the large eddy observed in this visualization.

which have the same flow conditions, i.e. the same  $Re$  and  $S$ , the impact of PVC on the overall entrainment process will be brought into sharp focus.

It has been found that, by introducing a localized combustion region in a strongly swirling jet, the PVC motions are substantially reduced. In a previous work [1], the PVC was shown to be excited by high-frequency, intense premixed combustion; it was also demonstrated that PVC was damped out considerably under diffusive combustion because of large density gradients developed in the flow field. Visualization and velocity fluctuation monitoring in Fig. 8 clearly showed that, when a small flame was installed at the center of swirl jet, appreciable reductions were achieved in the intensity of large scale motions. As asserted earlier, this indicates that PVC motion has been substantially suppressed by introducing a small flame; this is believed to stem from the presence of localized density gradients. In comparison to the isothermal case (Fig. 7) where no combustion zone is present, the spreading angle of swirl jet is ostensibly decreased by the introduction of a localized com-

bustion zone (Fig. 8). Also, periodic signals in the velocity fluctuation are not observed. These provide convincing evidence to the argument that PVC has effectively been suppressed by the presence of a small



**Isothermal Swirling Jet with local combustion**

FIG. 8. Schlieren photographs and velocity signals of swirling jet with local combustion. Conditions are  $Re = 20\,500$  and  $S = 1.87$ .

flame although they have the identical flow conditions.

In connection with the suppression of PVC by using a small propane flame, we should note that measurements of velocity alone could lead to inaccurate conclusions, since the flow field is not strictly isothermal. However, in the present study, the amount of fuel supplied in the center of the jet to maintain the flame is very minute (fuel flow rate is  $0.4 \text{ l min}^{-1}$ ). Consequently, the difference in the temperatures of the fluid in the swirl jet and of the surroundings is negligibly small. The hot wire probe is located on the time-averaged interface between the swirl jet and the surrounding air. Owing to these elaborate precautions taken in the experiment, the measured velocity signal is adopted in order to discern only whether the PVC motions in the flow field are present or not.

Now, we are in a position to assess quantitatively the impact of large and frequent engulfments in the mixing layer on the entrainment. So the crucial task is to secure accurate measurements of the entrainment.

### 3.2. Entrainment measurement

In order to establish the reliability and accuracy of the measurement technique of the present study, comparisons were attempted between the present results and the existing data of other works. For swirling flows, direct comparisons are extremely difficult; there usually are significant differences in the results available in the literature, such as the discrepancies in geometrical configuration and the methods adopted to generate swirl. However, comparisons can be made for a non-swirling free jet with nearly the same inlet conditions. The majority of the preceding measurements of the entrainment were carried out in the fully developed region for a convergent-nozzle non-swirling jet. These results are in reasonable agreement with the present data. Figure 9 shows such favorable com-

parisons with the results of Trabold *et al.* [12], which used the integration method for a tube-type nozzle with an end plate, and with those of Hill [13], which utilized the porous-wall technique of Ricou and Spalding [14]. The data of Trabold *et al.* [12] were acquired for a tube-type nozzle with a sharp edge similar to that adopted in the present experiment. Furthermore, the Reynolds number of Trabold *et al.* [12] was  $Re = 22\,000$ , which is very close to the value of the present study ( $Re = 20\,500$ ). Hill's data [13] were obtained for a convergent nozzle, but they are believed to be of high accuracy, and, therefore, they are selected for explicit comparisons with the present measurements.

Trabold *et al.* [12] show that the length of the tube type nozzle has a measurable influence on the entrainment rate; the tendency is that the entrainment rate is higher when this length is reasonably small. It is also important to recall that, in the nozzle exit region, the entrainment characteristics are sensitive to the geometry of the nozzle exit. In the present experiment, the length of the nozzle exit is approximately 2.5 nozzle diameters; this is well within the experimental ranges of Trabold *et al.* [12]. With respect to Hill's results [13], it should be mentioned that their experiments were performed for a convergent nozzle; consequently, the entrainment rates are anticipated to be lower than those conducted for a sharp-edged nozzle. In light of the above considerations, comparisons of the present results against these available data prove to be encouraging, as illustrated in Fig. 9.

In order to gain further insight into the effect of swirl on entrainment, the variations of the non-dimensionalized entrainment ( $\Psi$ ) with the axial distance ( $x/D$ ) from the nozzle exit are plotted in Fig. 10. As remarked previously, the entrainment increases as the swirl number increases. It is noteworthy that the linearity of entrainment rate becomes more prominent with  $S$  even in the initial regions. This observation is supported by the experimental findings of Crow and Champagne [15], where the jets forced by an external periodic surging generate large coherent structures in the flow boundary in the initial region. The entrainment rate varies quite linearly with the axial distance even in the initial region, and this is similar to the behavior in the fully developed region.

Next, the effect of the Reynolds number on the entrainment process is delineated, as illustrated in Fig. 11. In the case of a weakly swirling jet (see Fig. 11(a) for  $S = 0.25$ ), the influence of  $Re$  is minor, and  $\Psi$  tends to increase more or less non-linearly with  $x/D$  in the initial region. As can be seen in Fig. 6, the PVC motions are not discernible for this case ( $S = 0.25$ ). The observations obtainable in Fig. 11(a) are qualitatively similar to the case of conventional non-swirling free jet. On the contrary, for a strongly swirling jet (see Fig. 11(b) for  $S = 0.97$ ),  $\Psi$  increases as  $Re$  increases, and this dependence is appreciable. The behavior of  $\Psi$  with  $x/D$  is fairly linear over the range

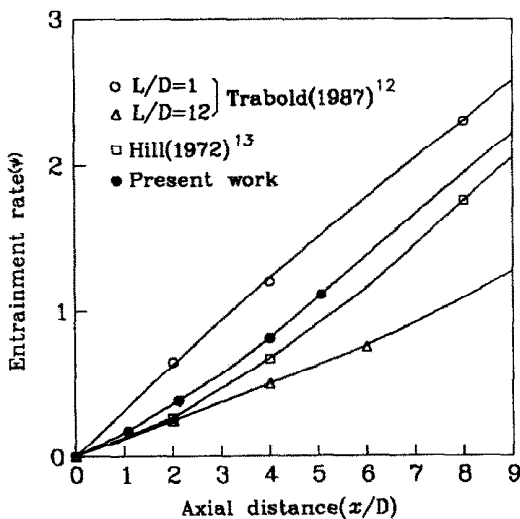


FIG. 9. Entrainment measurements of free non-swirling jets.

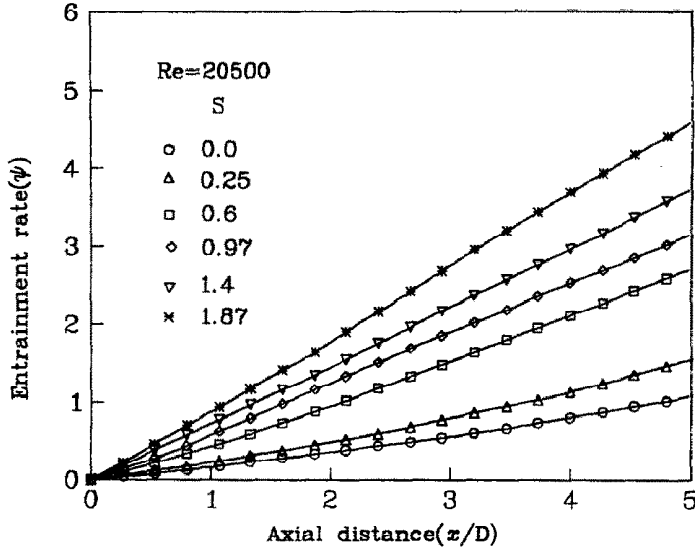


FIG. 10. Variations of entrainment rates with the axial distance ( $x/D$ ).

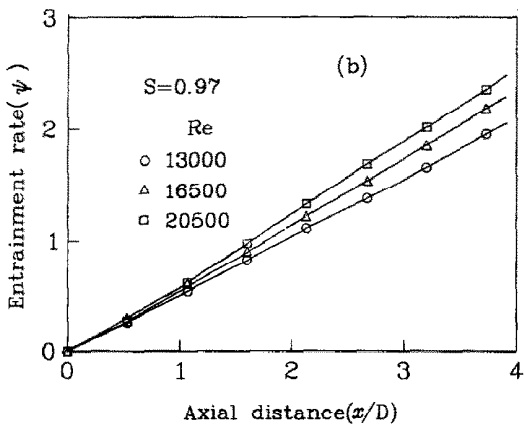
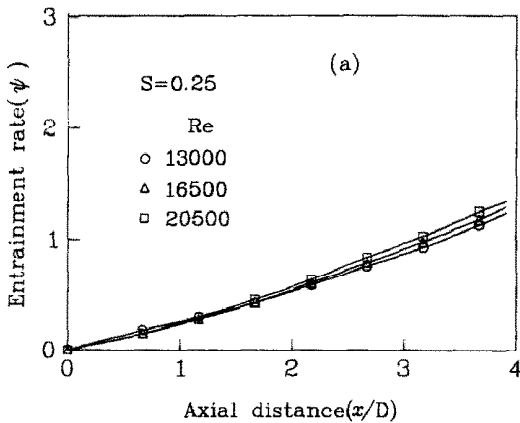


FIG. 11. Variations of entrainment rates with the Reynolds number ( $Re$ ). (a) A weakly swirling jet ( $S = 0.25$ ). (b) A strongly swirling jet ( $S = 0.97$ ).

from the nozzle exit to the downstream region. For this case ( $S = 0.97$ ), the PVC motions are notable. Figure 6(b) clearly demonstrates that, as  $Re$  increases, the intensity and frequency of the PVC motions increase. This is responsible for the increase of  $\Psi$  with  $Re$ .

We now need to clarify, in more quantitative terms, how the PVC affects the entrainment processes. Toward this end, measurements were taken of the entrainment rates of two swirl jets shown in Figs. 7 and 8. As stipulated earlier, careful selections are made of the data sets which satisfy the approximate relationship  $R_i V_i \cong R_{i+1} V_{i+1}$  and which are located nearest to the boundary of flow field. These data points are used to calculate the entrainment (see the thick solid line in Fig. 4). Summarizing such exercises, Fig. 12 was constructed to display the entrainments for the two representative swirling jets. It is immediately evident that the entrainment is substantially larger for the jet with the PVC than for the jet without the PVC. An important conclusion from Fig. 12 is that the PVC indeed plays a decisive role in promoting the entrainment.

Figure 13 presents the variations of the entrainment with the swirl number at several positions downstream of the nozzle exit for  $Re = 20500$ . It is stressed that the PVC motion was always observed if  $S > 0.6$  for all the Reynolds numbers in the present experiments when the swirl generator was used. It is discernible in Fig. 13 that the entrainment rate increases rapidly as  $S$  increases beyond approximately  $S \cong 0.6$ . Noting that  $S > 0.6$  indicates the range of the occurrence of the PVC, a significant implication follows from the results shown in Fig. 13. Based on these experimental findings, it can be asserted that the entrainment is indeed enhanced substantially by the large-scale

motions, which are maintained by the PVC. Furthermore, this enhancement of the entrainment is more pronounced in regions further downstream. A plausible physical argument is that the large-scale motions, which are generated in the close vicinity of the nozzle exit, cause the flow boundary to widen substantially in the downstream regions. This has direct influence in promoting the entrainment rate.

#### 4. CONCLUSIONS

The flow visualization studies have clearly established that swirl induces large-scale motions in the near exit region, which, in turn, give rise to substantial enhancements of the entrainment of surrounding air. The PVC phenomenon, which is excited in the case of strongly swirling jets ( $S > 0.6$ ), is found to be the principal mechanism in generating large eddy motions. In summary, the large-scale eddy motions, which are triggered by the presence of PVC, play a

dominant role in promoting the entrainment rate of the swirling jet.

In an effort to probe into the physical mechanisms at work, a new technique to measure the entrainment rate has been devised. Two representative swirling jets, one with a PVC and the other with a substantially suppressed PVC, were employed for quantitative evaluations. The results of such direct measurements of the entrainment are fully supportive of the above-stated contentions. For the weakly swirling jet ( $S < 0.6$ ), the entrainment rate is fairly independent of the Reynolds number; the entrainment rate varies more or less non-linearly in the initial exit region of the jet. For the strongly swirling jet ( $S > 0.6$ ) with a PVC, the shedding frequency of large-eddy structures increases with the Reynolds number; consequently the entrainment rate increases as the Reynolds number increases. Also, the entrainment rate varies nearly linearly with the downstream distance even in the initial region soon after the nozzle exit. The rate of increase of the entrainment is noticeably large as the swirl number  $S$  crosses over a threshold value  $S \cong 0.6$ ; an intense PVC is known to be developed when  $S > 0.6$ , and this finding provides further evidence to the decisive influence that PVC exerts on enhancing the entrainment.

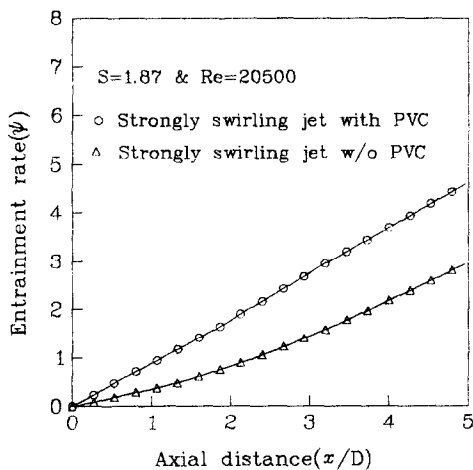


FIG. 12. Comparisons of the entrainment rates of a swirling jet with PVC and of a swirling jet without PVC.  $Re = 20\,500$  and  $S = 1.87$ .

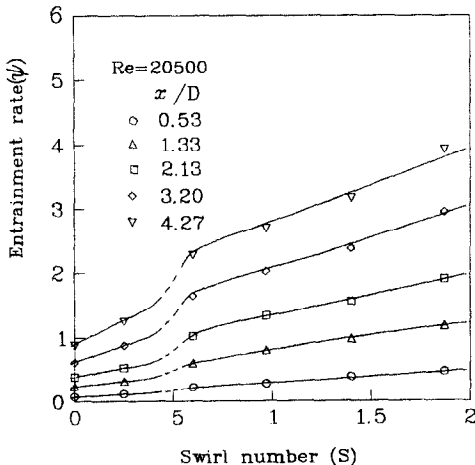


FIG. 13. Variations of the entrainment rates with swirl numbers.

#### REFERENCES

1. A. K. Gupta, D. G. Lilley and N. Syred, *Swirl Flows*. Abacus Press, London (1984).
2. R. C. Chanaud, Observations of oscillatory motion in certain swirling flows, *J. Fluid Mech.* **21**, 111–127 (1965).
3. R. M. Bevilacqua and P. S. Lykoudis, Some observations on the mechanism of entrainment, *AIAA J.* **15**, 1194–1196 (1977).
4. W. Leuckel and N. Fricker, Characteristics of swirl stabilized natural gas flames, *J. Inst. Fuel* **49**, 103–112 (1976).
5. J. M. Beer and N. A. Chigier, *Combustion Aerodynamics*. Applied Science Publishers, London (1972).
6. M. A. Delichatsios and L. Orloff, Entrainment measurements in turbulent buoyant jet flames and implications for modeling, *21st Symp. (Int.) on Combust.*, pp. 367–375 (1984).
7. W. G. Rose, A swirling round turbulent jet, *J. Appl. Mech.* **29**, 615–625 (1962).
8. N. M. Kerr and D. Fraser, Swirl Part 2: Effect on flame performance and modeling of swirling flames, *J. Inst. Fuel* **38**, 519–538 (1965).
9. N. A. Chigier and J. M. Beer, Velocity and static pressure distribution in swirling air jets, *J. Basic Engng* **86**, 788–798 (1964).
10. M. V. Dyke, *An Album of Fluid Motion*, Fig. 171. The Parabolic Press, California (1982).
11. R. J. Moffat, Describing the uncertainties in experimental results, *Exp. Thermal Fluid Sci.* **1**, 3–17 (1988).
12. T. A. Trabold, E. B. Esen and N. T. Obot, Entrainment by turbulent jets issuing from sharp-edged inlet round nozzles, *J. Fluid Engng* **109**, 248–254 (1987).
13. B. J. Hill, Measurement of local entrainment rate in the initial region of axisymmetric turbulent air jets, *J. Fluid Mech.* **51**, 773–779 (1972).
14. F. P. Ricou and D. B. Spalding, Measurements of entrainment by axisymmetrical turbulent jets, *J. Fluid Mech.* **11**, 21–32 (1961).
15. S. C. Crow and F. H. Champagne, Orderly structure in jet turbulence, *J. Fluid Mech.* **48**, 547–591 (1971).